J. Space Weather Space Clim. 2023, **13**, 22
© A. Mishev et al., Published by EDP Sciences 2023
https://doi.org/10.1051/swsc/2023020

JSWSC
Available online at:
www.swsc-journal.org

Topical Issue - Space Climate: Long-term effects of solar variability on the Earth's environment

Research Article — Open Access

Assessment of the radiation risk at flight altitudes for an extreme solar particle storm of 774 AD

Alexander Mishev[1,2,*], Sanja Panovska[3], and Ilya Usoskin[1,2]

[1] Space Physics and Astronomy Research Unit, University of Oulu, Pentti Kaiteran katu 1, 90570 Oulu, Finland
[2] Sodankylä Geophysical Observatory, University of Oulu, Tähteläntie 62, 99600 Sodankylä, Finland
[3] GFZ German Research Centre for Geosciences, Helmholtz Centre Potsdam, Wissenschaftpark "Albert Einstein", Telegrafenberg, 14473 Potsdam, Germany

Received 21 March 2023 / Accepted 28 July 2023

Abstract – Intense solar activity can lead to an acceleration of solar energetic particles and accordingly increase in the complex radiation field at commercial aviation flight altitudes. We considered here the strongest ever reported event, namely that of 774 AD registered on the basis of cosmogenic-isotope measurements, and computed the ambient dose at aviation altitude(s). Since the spectrum of solar protons during the 774 AD event cannot be directly obtained, as a first step, we derived the spectra of the solar protons during the ground level enhancement (GLE) #5 on 23 February 1956, the strongest event observed by direct measurements, which was subsequently scaled to the size of the 774 AD event and eventually used as input to the corresponding radiation model. The GLE #5 was considered a conservative approach because it revealed the hardest-ever derived energy spectrum. The global map of the ambient dose was computed under realistic data-based reconstruction of the geomagnetic field during the 774 AD epoch, based on paleomagnetic measurements. A realistic approach on the basis of a GLE #45 on 24 October 1989 was also considered, that is by scaling an event with softer spectra and lower particle fluxes compared to the GLE #5. The altitude dependence of the event-integrated dose at altitudes from 30 kft to 50 kft (9.1–15.2 km) was also computed for both scenarios. Our study of the radiation effects during the extreme event of 774 AD gives the necessary basis to be used as a reference to assess the worst-case scenario for a specific threat, that is radiation dose at flight altitudes.

Keywords: Extreme solar energetic particle events / 774 AD event / Neutron monitors / Radiation environment

1 Introduction

An omnipresent flux of subatomic particles in the vicinity of the Earth, that is cosmic rays (CRs) constantly enter the Earth's atmosphere. It is composed mostly of protons, α-particles, and a small amount of heavier nuclei, with their energy ranging from about 10^6 to 10^{21} eV/n and following a nearly power-law distribution in the energy spectrum (e.g. Gaisser et al., 2016; Beatty et al., 2018, and references therein). The deka-MeV kinetic energy particles are absorbed in the upper atmosphere. On the other hand particles with kinetic energy of about hundred MeV and GeV range produce secondaries following consecutive interactions with the medium constituents when entering the atmosphere. In such a way, each collision adds the next generation of particles, producing a complicated nuclear-electromagnetic-muon cascade known as an extensive air shower (for details see Dorman, 2004; Grieder, 2011, and references therein). Hence, the CRs, specifically those originating from the Galaxy, called galactic cosmic rays (GCRs), determine the complex radiation field in the atmosphere, particularly at aviation flight altitudes. The GCR flux is slightly modulated in the heliosphere, responding in anti-correlation to the 11-year solar cycle (e.g. Potgieter, 2013, and references therein). The GCR flux, respectively the radiation field at aviation altitudes, are impacted by transients and disturbances in the heliosphere, due to coronal mass ejections (CMEs) and corotating interaction regions of the solar wind, leading to the so-called Forbush decreases (Forbush, 1937; Belov, 2009). In addition, taking into account that CRs are charged particles, therefore experience the Lorentz force when propagating in a magnetic field, the geomagnetosphere deflects part of the incoming CRs preventing them from penetrating the atmosphere, yet during geomagnetic storms, the cutoff rigidity is usually reduced, leading to a small increase of incident CRs, and thus the atmospheric radiation environment. This particularly affects low and mid-latitudes, being more sensitive to changes in cutoff rigidity than the high latitudes, where the geomagnetospheric deflection is anyway marginal.

*Corresponding author: alexander.mishev@oulu.fi

While the GCR flux is slightly variable, resulting in a quasi-constant radiation field in the atmosphere, the situation could change dramatically during solar energetic particle (SEP) events. Solar eruptions, viz. solar flares and/or CMEs can accelerate solar ions to high energies, known as SEPs (e.g. Cliver et al., 2004; Desai & Giacalone, 2016, and references therein). The energy of SEPs is in the deka-MeV range in most cases, and sometimes in the 100-MeV kinetic energy range, but rarely, SEPs can be accelerated to the GeV/n range. When the kinetic energy of SEPs is ≈300 MeV or about 433 MeV for the high-mountain polar region and sea level respectively (for details see Mishev & Poluianov, 2021), the secondaries produced in the particle shower can reach the ground, eventually registered by ground-based detectors such as neutron monitors (NMs – see, e.g. Hatton, 1971; Simpson, 2000). Such type of events is called ground-level enhancements (GLEs – e.g., Shea & Smart, 1982; Aschwanden, 2012; Poluianov et al., 2017).

Despite GLEs being relatively rare compared to the bulk of solar particle events, occurring only several times per solar cycle (Shea & Smart, 2000, 2012), they represent a significant space weather thread (e.g. Schwenn, 2006; Pulkkinen, 2007; Miroshnichenko, 2018, and references therein). High-energy SEPs can degrade electronic components in space missions and none the least pose an increased radiation threat to astronauts as well as aircrews, specifically during transpolar flights for the latter (e.g. Vainio et al., 2009, and references therein).

Here we focus on a very specific type of event, called extreme solar particle events (ESPEs) that produce such an enormous amount of cosmogenic isotopes that they can be measured via their signatures in natural archives over the past millennia (for details see Usoskin, 2017; Miyake et al., 2019; Cliver et al., 2022, and references therein). In this study, we consider the strongest ever recorded such type of event: the 774 AD SEP (Miyake et al., 2012; Cliver et al., 2022). On the basis of recent reconstructions and corresponding scaling based on extensive Monte Carlo simulations (Usoskin et al., 2020b), and a realistic reconstruction of the geomagnetic field during that epoch, based on paleomagnetic measurements, we assessed the radiation dose at flight altitudes during this historical extreme event using two different approaches: a conservative i.e. worst case scenario, and a realistic one. As a first step, we derived the SEP spectra of GLE #5 and GLE #45 (Section 2) using after scaling as inputs for the corresponding radiation dose model (Section 3). Then we computed accordingly the ambient dose at several altitudes during the 774 AD event employing a reconstructed geomagnetic field at the epoch.

2 GLEs and the 774 AD event

At present the only known way to find a notable signature of extreme SEP event that occurred in the past is based on cosmogenic isotopes measurements, that is by radiocarbon (^{14}C; half-life = 5.73 × 10^{3} years), Beryllium-10 (^{10}Be; halflife = 1.36 × 10^{6} years), and Chlorine-36 (^{36}Cl; halflife = 3.01 × 10^{5} years) imprints. These radionuclides are produced following secondary CR interactions with the atmospheric constituents, namely neutron capture ^{14}N(n,p)^{14}C for the radiocarbon, spallation of Oxygen and Nitrogen nuclei by secondary energetic particles for ^{10}Be, and spallation of ^{40}Ar for the Chlorine. While the background of cosmogenic radionuclides is determined by the omnipresent flux of GCRs (e.g. Lingenfelter & Ramaty, 1970; Castagnoli & Lal, 1980), extreme SEP events may also provide their signatures in the isotope records, namely by the secondary particle interactions (e.g. Usoskin, 2017; Usoskin & Kovaltsov, 2021; Cliver et al., 2022).

Up to now, the largest SEP event identified on the basis of cosmogenic-isotope records is the 774 AD event discovered by Miyake et al. (2012), also confirmed by other teams by various cosmogenic isotopes measurements including both hemispheres (e.g. Usoskin et al., 2013; Jull et al., 2014; Sukhodolov et al., 2017; Uusitalo et al., 2018). At present, considering the latitudinal gradient and inferred global symmetry of the cosmogenic signal, the response in ^{10}Be and none the least the identification of similar cosmogenic nuclide events, suggest the SEP origin as a plausible scenario (for details see the discussion in Usoskin et al., 2013; Usoskin & Kovaltsov, 2021; Cliver et al., 2022, and the corresponding references therein).

Naturally, in order to assess space weather effects during the 774 AD SEP event, it is necessary to possess reliable information about the spectra of the incoming CR particles, as well as the magnetospheric field at the epoch. We emphasize that the strongest directly recorded event, the GLE #5 on 23 February 1956, is not large enough to produce a notable cosmogenic isotope signal, yet it is used as a reference (Usoskin et al., 2020b). Taking into account that SEP event magnitude correlates with the spectrum hardness, that is, stronger events reveal hard spectra (Asvestari et al., 2017), and that the 23 February 1956 event exhibited one of the hardest spectra for the directly recorded events (Vashenyuk et al., 2006; Tuohino et al., 2018), we derived the spectra of the latter (discussed below) and scaled to the 774 AD event. However, the realistic spectrum of the ESPE of 774 AD might have been softer than that of GLE#5 (Koldobskiy et al., 2023), and accordingly, we also considered an event with a softer SEP spectrum, that is GLE #45 on 24 October 1989 (for details see their Fig. 49 in Cliver et al., 2022; Koldobskiy et al., 2023).

For the analysis of GLE #5, we employed a method based on the modeling of the global NM network response and optimization of the model parameters describing the SEP spectra and anisotropy, over the experimental NM count rate increases. The method is adopted from the study by Cramp et al. (1997), details and applications are given elsewhere (Mishev et al., 2018b, 2021a, 2022b).

The response of each NM used in the analysis is computed by an integral of the product of the primary CR spectrum $J(P, t)$ with the NM yield function $S(P, h)$, that is the count rate of an NM at a given altitude (atmospheric depth) h and time t is expressed as:

$$N(P_{\rm c}, h, t) = \sum_i \int_{P_{\rm c}}^{\infty} S_i(P, h) J_i(P, t) \mathrm{d}p, \qquad (1)$$

where $P_{\rm c}$ is the local geomagnetic cutoff rigidity (e.g. Cooke et al., 1991), h is the atmospheric depth (or altitude), $S_i(P, h)$ [m^2 sr] is the NM yield function for primaries of particle type i (protons and/or α-particles), $J_i(P, t)$ [GV m^2 sr sec]$^{-1}$ is the rigidity spectrum of the primary particle of type i at time t (Clem & Dorman, 2000).

The unfolding is performed using the numerical method by Levenberg (1944) and Marquardt (1963) with additional regularization (Aleksandrov, 1971; Golub & Van Loan, 1980; Mishev et al., 2005), resulting in a robust selection of the final solution, that is solution corresponding to the global minimum (for details see Himmelblau, 1972; Tikhonov et al., 1995; Aster et al., 2005, and the discussions therein). The method was recently verified by direct space-borne measurements (for details see Mishev et al., 2021b; Koldobskiy et al., 2021; Koldobskiy & Mishev, 2022). We emphasize that NM yield function employed for the present analysis (Mishev et al., 2020) was verified by latitude surveys, direct space-borne records by PAMELA (Payload for Antimatter Matter Exploration and Light-nuclei Astrophysics, Adriani et al., 2017) and AMS-02 (Alpha Magnetic Spectrometer – Aguilar et al., 2021), more details are given elsewhere (Nuntiyakul et al., 2018; Koldobskiy et al., 2019; Mishev et al., 2020).

Using de-trended records retrieved from the GLE database (Usoskin et al., 2020a), and the method described in Mishev (2023), we assessed the spectra and angular distribution of SEPs during the GLE #5, where the best fit of the derived spectra was achieved using a modified power-law:

$$J_{||}(P) = J_0 P^{-(\gamma+\delta\gamma(P-1))}, \qquad (2)$$

where the flux of particles with rigidity P in [GV] is along the axis of symmetry of arriving SEPs, the power-law exponent is γ with the steepening of $\delta\gamma$.

Accordingly, the angular distribution, that is the pitch angle distribution (PAD) was approximated with Gaussian:

$$G(\alpha(P)) \sim \exp(-\alpha^2/\sigma^2), \qquad (3)$$

where α is the pitch angle, σ accounts for the width of the distribution. While earlier estimates (e.g., Usoskin et al., 2020b) were based on an explicit assumption of the isotropic SEP flux for GLE #5, here we used a more realistic reconstruction considering also the angular distribution of SEPs.

The derived spectra and anisotropy of SEPs during GLE #5 for selected periods of the event are presented in Figure 1, the details are given in Table 1. We emphasize that the SEP spectra during GLE #5 remained hard throughout the whole event and revealed significant flux (for details see Vashenyuk et al., 2006, 2008, and the comparison with other events therein).

Similarly, we derived the SEP spectra during another event used for the scaling to the 774 AD event, namely GLE #45 on 24 October 1989, depicted in Figure 2, the details are given in Table 2.

We note, that in this case the angular distribution is approximated with a more complicated shape, which accounts for particles arriving from the anti-sun direction:

$$G(\alpha(P)) \sim \exp(-\alpha^2/\sigma_1^2) + B \times \exp(-(\alpha-\pi)^2/\sigma_2^2), \qquad (4)$$

where α is the pitch angle, σ_1 and σ_2 are parameters corresponding to the width of the pitch angle distribution, B is a parameter corresponding to the contribution of the particle flux arriving from the anti-sun direction.

We note that during the unfolding, we derived simultaneously the SEP spectra and PAD, the latter important to obtain as realistically as possible the former (for details see Cramp et al., 1997, and the discussion therein), however, the derived PADs are not used for the subsequent computations of the space weather effects as discussed below. Both events had relatively hard SEP spectra. In most cases the SEP spectra during GLEs gradually softened throughout the events (e.g. Vashenyuk et al., 2008; Tuohino et al., 2018, and references therein), which is the case for GLE #45, yet during GLE #5, they remained hard during the whole event. In both events the particle flux rapidly increased, reaching a maximum and thereafter gradually decreased.

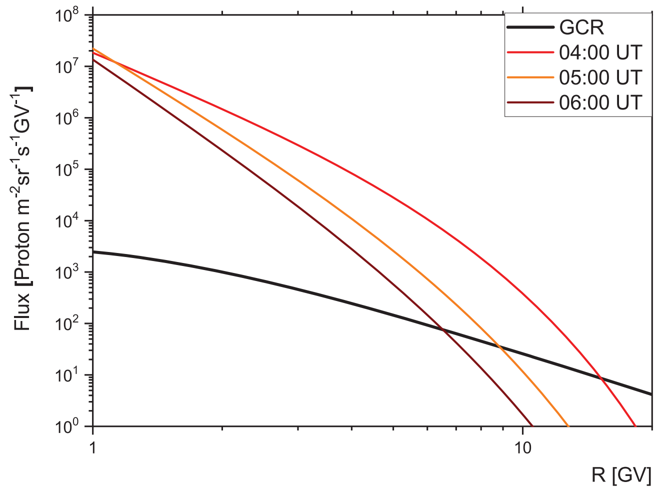

Figure 1. Derived SEP spectra during peak stage of GLE #5 (23 February 1956).

Table 1. Derived spectral and angular characteristics of the GLE #5. The columns correspond to the integration interval, particle flux J_0, spectrum slope γ, steepening of the spectrum $\delta\gamma$, width of the PAD σ^2 (see Eqs. (2) and (3)).

Integration interval UT	J_0 [$m^{-2}s^{-1}sr^{-1}GV^{-1}$]	γ	$\delta\gamma$	σ^2 [rad^2]
04:00–04:05	1.8391E7	3.51	0.13	0.26
04:10–04:15	7.582E7	4.0	0.13	0.45
05:00–05:05	2.22E7	5.11	0.13	0.97
06:00–06:05	1.35E7	5.73	0.13	2.4
07:00–07:05	1.1E7	6.03	0.12	2.4
10:00–11:00	4.62E6	6.5	0.11	2.6
12:00–13:00	3.54E6	6.8	0.1	2.7

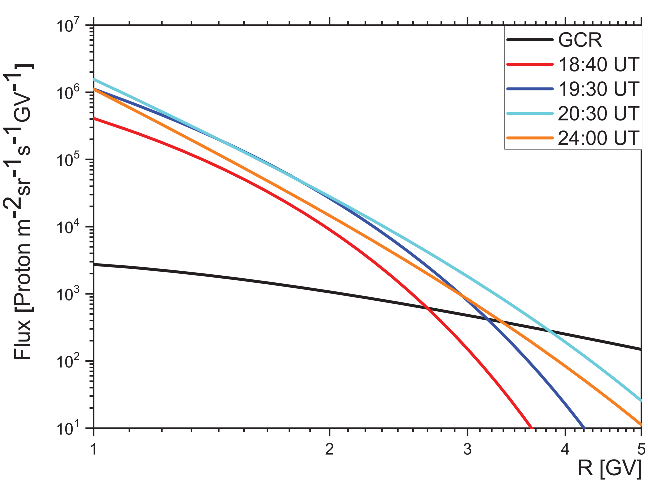

Figure 2. Derived SEP spectra during various stages of GLE #45.

Table 2. Derived spectral and angular characteristics of GLE #45 (24 October 1989). The columns correspond to the integration interval, particle flux J_0, spectrum slope γ, steepening of the spectrum $\delta\gamma$, width of the PAD for particles arriving from sunward direction σ_1^2, the contribution of the particles from anti-sunward direction B and their PAD width σ_2^2.

Integration interval UT	J_0 [$m^{-2}s^{-1}sr^{-1}GV^{-1}$]	γ	$\delta\gamma$	σ_1^2 [rad^2]	B	σ_2^2 [rad^2]
18:40–18:45	4.1E5	3.8	1.7	1.1	0.05	1.2
19:30–19:35	1.12E6	4.2	1.2	1.6	0.3	1.7
20:30–20:35	1.56E6	5.45	0.35	3.4	0.7	3.0
21:45–22:00	1.31E6	5.64	0.33	3.45	0.72	3.2
00:00–01:00	1.11E6	5.95	0.3	3.6	0.71	3.5
02:00–03:00	7.8E5	6.1	0.27	3.8	0.7	3.7

Hereby, we derived the spectra of two GLEs, namely GLE #5, revealing the hardest ever observed spectra, used as a conservative approach after scaling to 774 AD event, and GLE #45, with softer spectra, used as realistic approach, accordingly. We emphasize that only SEPs with energy greater than about 200 MeV/n can contribute to the enhancement of the radiation field at flight altitudes (e.g. Ferrari et al., 2001; Spurny et al., 2002; Matthiä et al., 2008; Mertens et al., 2013; Paschalis et al., 2014).

3 CRAC:DOMO radiation model

For the computation of the ambient dose during the 774 AD event we employed the updated radiation model Oulu CRAC: DOMO (Cosmic Ray Atmospheric Cascade: Dosimetric Model) (Mishev & Usoskin, 2015) and scaling of the effective dose to ambient dose H*, the latter recommended as new operational dose quantity, according to Matthiä et al. (2022). The model is based on precomputed yield functions of the radiation dose (e.g. Hands et al., 2022), obtained by Monte Carlo simulations with a GEANT 4 based tool PLANETOCOSMICS (Agostinelli et al., 2003; Desorgher et al., 2005), that is a response matrix over a layered NRLMSISE-00 atmospheric model (Picone et al., 2002) giving the secondary particle flux and spectra as a function of altitude for a monoenergetic incident particles ranging in a logarithmic step from MeV up to TeV kinetic energy range, computed separately for protons and alphas. The full description and applications of the model including verification and comparison with other models and experimental data are given in (Meier et al., 2016, 2018; Mishev & Usoskin, 2018; Mishev et al., 2018a, 2021b, 2022a).

The dose rate (effective, ambient, ambient equivalent) at a given atmospheric altitude (depth) h induced by the ith component of CRs (proton or α-particle, the latter accounting effectively all heavy particles) is the integral of a product of the primary particle spectrum with the corresponding yield function:

$$E(h, T, \theta, \varphi) = \sum_i \int_{T(P_c)}^{\infty} \int_{\Omega} J_i(T) Y_i(T, h) \mathrm{d}\Omega(\theta, \varphi) \mathrm{d}T, \tag{5}$$

where $J_i(T)$ is the differential energy spectrum of the primary CR for the ith component and Y_i is the corresponding effective dose/ambient dose yield function. The integration is over the kinetic energy T above $T(P_c)$, the latter determined by the local cutoff rigidity P_c and over the solid angle Ω.

Accordingly, the effective/ambient dose yield function Y_i is a summation of the contributions from different secondary particles defined as:

$$Y_i(T, h) = \sum_j \int_{T^*} F_{i,j}(h, T, T^*, \theta, \varphi) Cj(T^*) \mathrm{d}T, \tag{6}$$

where $C_j(T^*)$ is the fluence to effective/ambient dose conversion coefficient for a secondary particle of type j (neutron, proton, γ, e^-, e^+, μ^-, μ^+, π^-, π^+) with energy T^*, $F_{i,j}(h, T, T^*, \theta, \varphi)$ is the fluence of secondary particles of type j, produced by a primary CR particle of type i (proton or α-particle) with given energy T arriving at the top of the atmosphere from zenith angle θ and azimuth angle φ. The employed fluence-to-dose conversion coefficients $C_j(T^*)$ are taken according to Pelliccioni (2000) and Petoussi-Henss et al. (2010) for the ambient dose equivalent and effective dose respectively.

We note that equivalent dose accounts for the stochastic health effects on the human body due low radiation levels, which explicitly considers the biological effectiveness of the radiation, namely the type and energy, whilst the effective dose represents the tissue-weighted sum of the equivalent doses. The effective dose E accounts for not only the type of radiation, but also the type of the organ or tissue being irradiated, and it is used for radiation protection purposes. Despite E is not a measurable quantity, it is usually estimated using models, whilst ambient dose equivalent H(10)* is measured with suitable detectors. Recently, a new quantity for assessment of the effective dose was proposed to replace H(10)*, which takes into account the energy and particle type, that is ambient dose H*, (for details see Matthiä et al., 2022, and the discussion therein), which we employ in this study.

For SEP events, the radiation dose is computed using equation (5) as a superposition of the GCRs contribution and solar protons contribution, the former obtained using the force field model (Caballero-Lopez & Moraal, 2004; Usoskin et al., 2005) with the local interstellar spectrum provided by Vos & Potgieter (2015) and modulation potential from Usoskin et al. (2017), while the latter is computed using the derived spectra for a given event, assuming pure proton mass composition (e.g. Reames, 2013, and references therein).

We would like to emphasize that despite the naturally derived anisotropy during strong SEP events, we conservatively assumed an isotropic angular distribution of the solar protons similar to Copeland et al. (2008) and Mishev & Usoskin (2018). We note that the use of the former generation conversion coefficients $C_j(T^*)$ by ICRP (1996) increased the assessed radiation dose of about 15–20%, yet considerably below the other model uncertainties (for details see Copeland & Atwell, 2019; Yang & Sheu, 2020, and the discussion therein). Besides, since the effective dose is not a conservative approach at flight altitudes, an aforementioned scaling to the new recommended operational dose quantity, that is ambient dose H* is performed similarly to Matthiä et al. (2022). Most radiation models developed in recent years (e.g. Matthiä et al., 2008; Latocha et al., 2009; Banjac et al., 2019; Hands et al., 2022), nicely agree with each other (e.g. for earlier versions see Bottollier-Depois et al., 2009, and references therein), however a significant discrepancy in the computation of the radiation dose during SEP events was shown to be predominantly due to the SEP spectra employed as input for the corresponding model (for details see Bütikofer & Flückiger, 2013). Therefore, it is important to possess precise SEP spectra, if possible derived with verified method(s) (e.g. Jiggens et al., 2019; Mishev & Jiggens, 2019), as in the study presented here.

4 Global mapsof ambient dose H* for the 774 AD event

For the computation of the ambient dose H* corresponding to the 774 AD event, we considered the derived spectra during GLE #5 (Table 1) with a scaling factor ≈100, as a conservative approach, and GLE #45 (Table 2), with a scaling factor ≈500 as a realistic approach. The scaling is selected so that the scaled event-integrated fluence is consistent with the measured cosmogenic production (Usoskin et al., 2020b; Cliver et al., 2022; Koldobskiy et al., 2023). Besides, we assumed that the cosmogenic production during 774 AD ESEP is due to a single event, (the other possibility is a sequence of events such as Halloween events or September–October 1989 (Humble et al., 1991; Cramp et al., 1997; Vashenyuk et al., 2006), not considered here), lasting 24 h and with a time profile similar to other strong events (Vashenyuk et al., 2008; Moraal & McCracken, 2012; Copeland and Atwell, 2019), namely following Tables 1 and 2 as a conservative approach, that is we considered the last derived spectra to remain unchanged till the end of the event. Then we employed the model described in Section 3, equation (5) following the scheme by Mishev (2023).

In addition, in order to model the effects of the GCRs background and the SEPs itself we assumed a moderately active Sun, that is with the modulation parameter of about 500 MV (Usoskin et al., 2021). Since both GCR and SEP are deflected by the geomagnetic field in the vicinity of Earth, we modelled realistically the geomagnetic field on the basis of recent archaeomagnetic reconstructions, namely we computed the effective geomagnetic cutoff rigidities on a step $1 \times 1°$ applying an eccentric dipole approximation (Nevalainen et al., 2013). Nowadays, the scientific community possesses paleomagnetic data from different sources e.g. archeological artifacts, volcanic and sediment data (e.g. Brown et al., 2015a, 2015b). In this study, we used a global geomagnetic field model covering the Holocene, CALS10k.2 (Constable et al., 2016). Details on the modeling approach and cutoff rigidity can be found in (Panovska et al., 2019; Gao et al., 2022).

The first computation was performed as a conservative approach i.e. by scaling 100-fold the spectra of the GLE #5

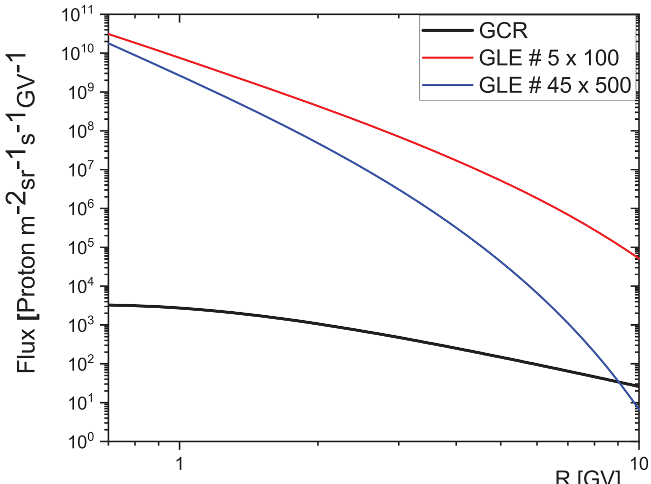

Figure 3. The spectra of GLE #5 and GLE #45 scaled to 774 AD as denoted in the legend, considered as a worst-case scenario and realistic scenario computation of the ambient dose, respectively.

(see Fig. 3), assuming an isotropic angular distribution similar to Copeland et al. (2008); Mishev & Usoskin (2018). As expected the radiation dose is maximal in the polar region. An illustration of the peak ambient dose, corresponding to GLE particles with maximal intensity is given in Figure 4. One can see that the ambient dose H* at 40 kft (12.2 km) above sea level (a.s.l.) is slightly below 1 Sv/h. We emphasize that the SEP spectra are highly variable (Moraal & McCracken, 2012). Hence, in most cases the radiation dose peaks on a short time scale (for details see the discussion in Spurny & Dachev, 2001; Matthiä et al., 2009; Al Anid et al., 2014; Mishev et al., 2021b). Therefore, for a realistic assessment of the radiation dose it is natural to perform computation over a period corresponding to the whole event or for a period corresponding to the flight duration, specifically in the polar region. Therefore, for the following computation, we explicitly considered the time variation of the SEP spectra similar to GLE #5 in Table 1.

In Figure 5, we present the distribution of the ambient dose H* over the globe at an altitude of 40 kft (12.2 km) a.s.l., integrated over the first 4 h of the modeled 774 AD event, considering the aforementioned assumptions. The altitude of 40 kft (≈12,192 m a.s.l.) is representative of a polar flight, while the 4-h period corresponds to the time span over the poles of a typical intercontinental flight. As expected, the radiation dose is maximal in the polar region, where the magnetospheric shielding is marginal. One can see that the ambient dose integrated over a selected period of 774 AD-like event would lead to severe effects including acute radiation syndrome (e.g. see chapter 18 in Kiefer, 1990).

Finally, we computed the event-integrated ambient dose H* over the globe at an altitude of 40 kft (12.2 km) a.s.l., employing the assumptions (GLE #5 spectra from Table 1, isotropic angular distribution) and 24 h duration of the event similar to other long-duration events (for details see Vashenyuk et al., 2008; Tuohino et al., 2018). In Figure A.1 in Appendix, we present the event-integrated distribution of the ambient dose H* over the globe at an altitude of 40 (12.2 km) kft a.s.l. Moreover, we also present the altitude dependence of the event-integrated H* ranging from 50 kft (15.2 km) a.s.l. to 30 kft (9.1 km) a.s.l.,

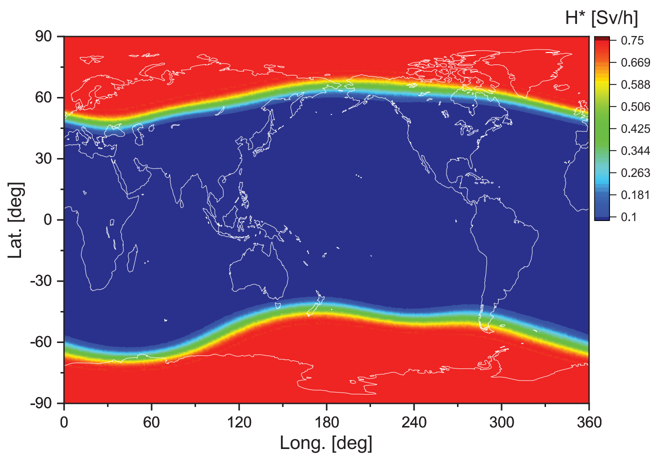

Figure 4. Global map of the ambient dose at altitude 40 kft (12.2 km) during the peak phase of 774 AD event, assuming worst case scenario.

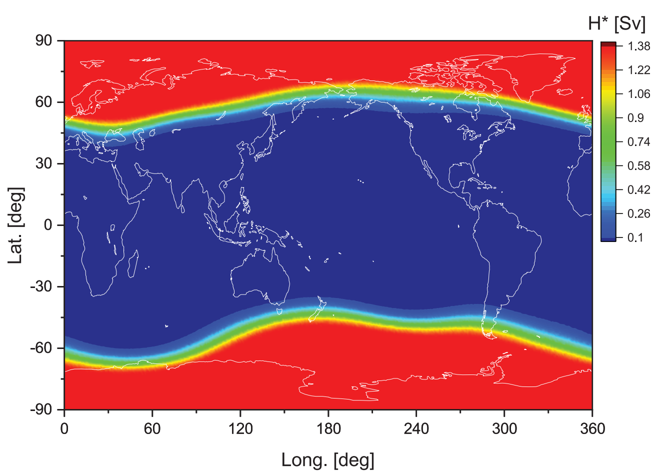

Figure 5. Global map of the integrated ambient dose at altitude 40 kft (12.2 km) over the first 4 h starting from the event onset during 774 AD event, assuming worst case scenario.

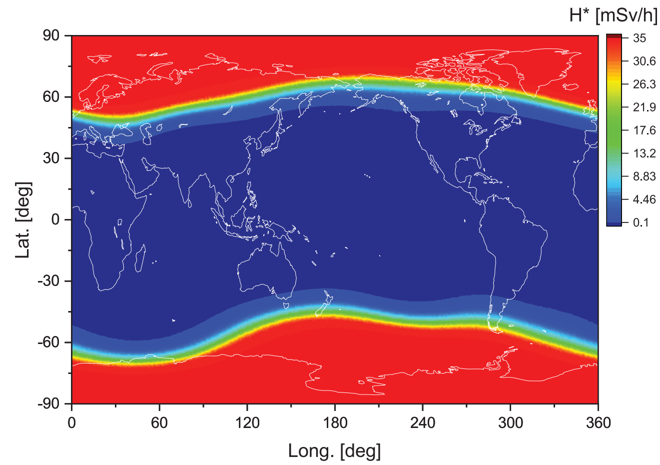

Figure 6. Global map of the ambient dose at altitude 40 kft (12.2 km) during the peak phase during 774 AD event, assuming realistic case scenario.

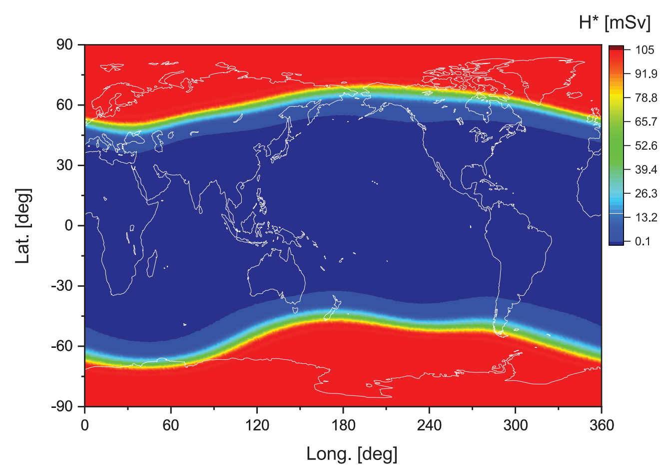

Figure 7. Global map of the integrated ambient dose at altitude 40 kft (12.2 km) over the first 4 h starting from the event onset during 774 AD event, assuming realistic case scenario.

given in the Supplementary material. One can see that the event-integrated H* significantly decreases as a function of altitude, ranging in the polar region from about 9.5 Sv at an altitude of 50 kft (15.2 km) a.s.l., 6 Sv at an altitude of 40 kft (12.2 km) a.s.l. and 2 Sv at an altitude of 30 kft (9.1 km) a.s.l., all representing significant threat.

The second computation was performed assuming a realistic scenario, that is softer spectra and scaling 500-fold the GLE #45 (Fig. 3), assuming similarly an isotropic angular distribution of the SEPs. The peak ambient dose, in this case, is considerably lower compared to the conservative approach, namely of about 35 mSv/h at an altitude of 40 kft (12.2 km) a.s.l. over the polar caps, details presented in Figure 6.

Accordingly, the distribution of the ambient dose H* over the globe at an altitude of 40 (12.2 km) kft a.s.l., integrated over the first four hours of 774 AD event, considering the realistic scenario is presented in Figure 7. One can see that the integrated radiation dose of about 100 mSv, can be harmful.

The event-integrated ambient dose H* over the globe at an altitude of 40 kft (12.2 km) a.s.l., assuming a realistic scenario (GLE #45 spectra from Table 2, isotropic angular distribution) and assuming 24 h duration of the event is given in Figure A.2. In this case, the event-integrated ambient dose H* ranges in the polar region from about 1.2 Sv at an altitude of 50 kft (15.2 km) a.s.l., 0.9 Sv at an altitude of 40 kft (12.2 km) a.s.l. and 0.3 Sv at an altitude of 35 kft (10.7 km) a.s.l., and drops below 0.1 Sv at an altitude of 30 kft (9.1 km) a.s.l. (for details see the Supplementary material).

Thus, in this section, we presented global maps of the peak, four hours integrated, and event-integrated ambient doses during the 774 AD extreme SEP event assuming the worst case, that is, very hard spectra, scenario and a realistic one with softer SEP spectra, lower flux. We also presented the altitude dependence of the event-integrated dose for both cases.

5 Conclusions

Study of the historical extreme SEP events, viz. events with cosmogenic-isotope imprints, specifically their possible terrestrial effects, including radiation dose at flight altitudes as considered in this study, allows one to assess the worst-case scenario during extreme events. Employing recent model studies and plausible assumptions related to event duration, spectral shape and non-the-least realistic reconstructions of the geomagnetic field during the epoch, we studied the possible impact of the 774 AD event. Here we assume that the 774 AD event was an ESPE (e.g. Usoskin & Kovaltsov, 2021; Cliver et al., 2022, and references therein). We assumed a single-event scenario, that is one event of the duration of 24 hours similar to the bulk of the strongest GLEs (Tuohino et al., 2018; Usoskin et al., 2020a), not considering a possible sequence of events such as September–October 1989 events (Humble et al., 1991) or Halloween events of October–November 2003 (Gopalswamy et al., 2005, 2012). Finally, we assumed moderate solar activity at the epoch of 774 AD and a conservative approach for the angular distribution of SEPs, which is isotropic, in order to assess the maximal radiation dose, considering the impossibility of obtaining any information about the PAD of SEPs during 774 AD. Here, we studied two scenarios: a conservative by employing hard spectra scaled from GLE #5, and a realistic one by employing softer spectra scaled from GLE #45.

We summarized the results as follows:

1. We derived SEP spectra for two strong GLEs, namely the strongest ever directly observed by ground-based NMs GLE #5 on 23 February 1956 and GLE #45 on 24 October 1989.
2. The cutoff rigidity during the 774 AD SEP event is computed with the greatest possible angular resolution of one degree, on the basis of paleomagnetic measurements, giving the necessary Gauss expansion coefficients and employing eccentric dipole approximation.
3. Using the reconstructed spectra and a 100-fold scaling of GLE #5 as a conservative approach and 500-fold of GLE #45 as a realistic approach, state-of-the-art model, and the computed cutoff rigidity, we calculated the global map of the peak ambient dose H*, the integrated over the first 4 h H* and the event-integrated H* at an altitude of 40 kft (12.2 km) during the 774 AD event.
4. The altitude dependence of the event-integrated dose ranging from 30 kft (9.1 km) to 50 kft (15.2 km) is presented in the Supplementary material.

The 774 AD ESPE considered in this study is the strongest ever reported on the basis of cosmogenic-isotope records. The event can be estimated conservatively by scaling with a factor of 100 the GLE #5 spectra, so that it can be used to assess the worst-case scenario for a specific threat, that is radiation dose at flight altitudes. The results presented in the article can serve a as reference for studying the worst-case scenario based on historical events, and the work opens a new window in space weather studies.

Acknowledgements. Part of this work was supported by the Academy of Finland (project 330063 QUASARE and 321882 ESPERA). The work was also supported by the HE program, project ALBATROS. This work was partially supported by the National Science Fund of Bulgaria under contract KP-06-H28/4. S. Panovska acknowledges the Discovery Fellowship at the GFZ Potsdam, Germany. The editor thanks two anonymous reviewers for their assistance in evaluating this paper.

Supplementary materials

The supplementary information of this article is available at https://www.swsc-journal.org/10.1051/swsc/2023020/olm.

Animation SA1. Event integrated ambient dose as function of the altitude assuming conservative scenario.

Animation SA2. Event integrated ambient dose as function of the altitude assuming realistic case scenario.

References

Adriani O, Barbarino GC, Bazilevskaya GA, Bellotti R, Boezio M, et al. 2017. Ten years of PAMELA in space. *Riv Nuovo Cimento* **40(10)**: 473–522. https://doi.org/10.1393/ncr/i2017-10140-x.

Agostinelli S, Allison J, Amako K, Apostolakis J, Araujo H, et al. 2003. GEANT4 – A simulation toolkit. *Nucl Instrum Methods Phys Res A* **506(3)**: 250–303. https://doi.org/10.1016/S0168-9002(03)01368-8.

Aguilar M, Ali Cavasonza L, Ambrosi G, Arruda L, Attig N, et al. 2021. The alpha magnetic spectrometer (AMS) on the international space station: Part II Results from the first seven years. *Phys Rep* **894**: 1–116. https://doi.org/10.1016/j.physrep.2020.09.003.

Al Anid H, Lewis B, Bennett L, Takada M, Duldig M. 2014. Aircrew radiation dose estimates during recent solar particle events and the effect of particle anisotropy. *Radiat Prot Dosim* **158(3)**: 355–367. https://doi.org/10.1093/rpd/nct234.

Aleksandrov L. 1971. The Newton-Kantorovich regularized computing processes. *USSR Comput Math Math Phys* **11(1)**: 46–57. https://doi.org/10.1016/0041-5553(71)90098-X.

Aschwanden M. 2012. GeV particle acceleration in solar flares and ground level enhancement (GLE) events. *Space Sci Rev* **171(1–4)**: 3–21. https://doi.org/10.1007/s11214-011-9865-x.

Aster R, Borchers B, Thurber C. 2005. *Parameter estimation and inverse problems*. Elsevier, New York. ISBN 0-12-065604-3.

Asvestari E, Willamo T, Gil A, Usoskin I, Kovaltsov G, Mikhailov V, Mayorov A. 2017. Analysis of ground level enhancements (GLE): Extreme solar energetic particle events have hard spectra. *Adv Space Res* **60**: 781–787. https://doi.org/10.1016/j.asr.2016.08.043.

Banjac S, Herbst K, Heber B. 2019. The atmospheric radiation interaction simulator (AtRIS): description and validation. *J Geophys Res Space Phys* **124(1)**: 50–67. https://doi.org/10.1029/2018JA026042.

Beatty J, Matthews J, Wakely S. 2018. Cosmic rays. In M. Tanabashi et al., review of particle physics, 424–432. *Phys Rev D* **98**: 030001. https://doi.org/10.1103/PhysRevD.98.030001.

Belov A. 2009. Forbush effects and their connection with solar, interplanetary and geomagnetic phenomena. *Proc Int Astron Union* **4(S257)**: 439–450. https://doi.org/10.1017/S1743921309029676.

Bottollier-Depois J, Beck P, Bennett B, Bennett L, Bütikofer R, et al. et al. 2009. Comparison of codes assessing galactic cosmic radiation exposure of aircraft crew. *Radiat Prot Dosim* **136(4)**: 317–323. https://doi.org/10.1093/rpd/ncp159.

Brown MC, Donadini F, Korte M, Nilsson A, Korhonen K, Lodge A, Lengyel SN, Constable CG. 2015a. GEOMAGIA50.v3: 1. General structure and modifications to the archeological and volcanic database recent advances in environmental magnetism and paleomagnetism. *Earth Planet Space* **67(1)**: 83. https://doi.org/10.1186/s40623-015-0232-0.

Brown MC, Donadini F, Nilsson A, Panovska S, Frank U, Korhonen K, Schuberth M, Korte M, Constable CG. 2015b. GEOMAGIA50.v3: 2. A new paleomagnetic database for lake and marine sediments. *Earth Planet Space* **67(1)**: 70. https://doi.org/10.1186/s40623-015-0233-z.

Bütikofer R, Flückiger E. 2013. Differences in published characteristics of GLE60 and their conseuences on computed radiation dose rates along selected flight paths. *J Phys Conf Ser* **409(1)**: 012166. https://doi.org/10.1088/1742-6596/409/1/012166.

Caballero-Lopez R, Moraal H. 2004. Limitations of the force field equation to describe cosmic ray modulation. *J Geophys Res* **109**: A01101. https://doi.org/10.1029/2003JA010098.

Castagnoli G, Lal D. 1980. Solar modulation effects in terrestrial production of carbon-14. *Radiocarbon* **22(2)**: 133–158. https://doi.org/10.1017/S0033822200009413.

Clem J, Dorman L. 2000. Neutron Monitor response functions. *Space Sci Rev* **93**: 335–359. https://doi.org/10.1023/A:1026508915269.

Cliver E, Kahler S, Reames D. 2004. Coronal Shocks and Solar Energetic Proton Events. *Astrophys J* **605**: 902–909. https://doi.org/10.1086/382651.

Cliver EW, Schrijver CJ, Shibata K, Usoskin IG. 2022. Extreme solar events. *Living Rev Solar Phys* **19(1)**: 2. https://doi.org/10.1007/s41116-022-00033-8.

Constable C, Korte M, Panovska S. 2016. Persistent high paleosecular variation activity in southern hemisphere for at least 10000 years. *Earth Planet Sci Lett* **453**: 78–86. https://doi.org/10.1016/j.epsl.2016.08.015.

Cooke D, Humble J, Shea M, Smart D, Lund N, Rasmussen I, Byrnak B, Goret P, Petrou N. 1991. On cosmic-ray cutoff terminology. *Il Nuovo Cimento C* **14(3)**: 213–234. https://doi.org/10.1007/BF02509357.

Copeland K, Atwell W. 2019. Flight safety implications of the extreme solar proton event of 23 February 1956. *Adv Space Res* **63(1)**: 665–671. https://doi.org/10.1016/j.asr.2018.11.005.

Copeland K, Sauer H, Duke F, Friedberg W. 2008. Cosmic radiation exposure of aircraft occupants on simulated high-latitude flights during solar proton events from 1 January 1986 through 1 January 2008. *Adv Space Res* **42(6)**: 1008–1029. https://doi.org/10.1016/j.asr.2008.03.001.

Cramp J, Duldig M, Flückiger E, Humble J, Shea M, Smart D. 1997. The October 22, 1989, solar cosmic enhancement: ray an analysis the anisotropy spectral characteristics. *J Geophys Res* **102(A11)**: 24237–24248. https://doi.org/10.1029/97JA01947.

Desai M, Giacalone J. 2016. Large gradual solar energetic particle events. *Living Rev Solar Phys* **13(1)**: 3. https://doi.org/10.1007/s41116-016-0002-5.

Desorgher L, Flückiger E, Gurtner M, Moser M, Bütikofer R. 2005. A Geant 4 code for computing the interaction of cosmic rays with the earth's atmosphere. *Int J Mod Phys A* **20(A11)**: 6802–6804. https://doi.org/10.1142/S0217751X05030132.

Dorman L. 2004. *Cosmic rays in the earth's atmosphere and underground*. Kluwer Academic Publishers, Dordrecht. ISBN 1-4020-2071-6.

Ferrari A, Pelliccioni M, Rancati T. 2001. Calculation of the radiation environment caused by galactic cosmic rays for determining air crew exposure. *Radiat Prot Dosim* **93(2)**: 101–114. https://doi.org/10.1093/oxfordjournals.rpd.a006418.

Forbush S. 1937. On the effects in cosmic-ray intensity observed during the recent magnetic storm. *Phys Rev* **51(12)**: 1108–1109.

Gaisser T, Engel R, Resconi E. 2016. *Cosmic rays and particle physics*. Cambridge University Press, Cambridge, UK. ISBN 9781139192194.

Gao J, Korte M, Panovska S, Rong Z, Wei Y. 2022. Geomagnetic field shielding over the last one hundred thousand years. *J Space Weather Space Clim* **12**: 31. https://doi.org/10.1051/swsc/2022027.

Golub G, Van Loan C. 1980. An analysis of the total least squares problem. *SIAM J Numer Anal* **17(6)**: 883–893.

Gopalswamy N, Barbieri L, Cliver E, Lu G, Plunkett S, Skoug R. 2005. Introduction to violent sun-earth connection events of October–November 2003. *J Geophys Res Space Phys* **110(A9)**: A09S00. https://doi.org/10.1029/2005JA011268.

Gopalswamy N, Xie H, Yashiro S, Akiyama S, Mäkelä P, Usoskin I. 2012. Properties of ground level enhancement events and the associated solar eruptions during solar cycle 23. *Space Sci Rev* **171(1–4)**: 23–60. https://doi.org/10.1007/s11214-012-9890-4.

Grieder P. 2011. *Extensive air showers: high energy phenomena and astrophysical aspects – a tutorial, reference manual and data book*, Springer, Space Science Library (Book 1009). ISBN 978-3540769408.

Hands A, Lei F, Davis C, Clewer B, Dyer C, Ryden K. 2022. A new model for nowcasting the aviation radiation environment with comparisons to in situ measurements during GLEs. *Space Weather* **20(8)**: e2022SW003155. https://doi.org/10.1029/2022SW003155.

Hatton C. 1971. The neutron monitor. In: *Progress in elementary particle and cosmic-ray physics X, Chap. 1*. North Holland Publishing Co., Amsterdam, pp. 3–100.

Himmelblau D. 1972. *Applied nonlinear programming*. McGraw-Hill, TX, USA. ISBN 978-0070289215.

Humble J, Duldig M, Smart D, Shea M. 1991. Detection of 0.5–15 GEV solar protons on 29 September 1989 at Australian stations. *Geophys Res Lett* **18(4)**: 737–740. https://doi.org/10.1029/91GL00017.

ICRP. 1996. ICRP Publication 74: conversion coefficients for use in radiological protection against external radiation. *Ann ICRP* **26(3–4)**: 1–205.

Jiggens P, Clavie C, Evans H, O'Brien T, Witasse O, et al. 2019. In situ data and effect correlation during September 2017 solar particle event. *Space Weather* **17(1)**: 99–117. https://doi.org/10.1029/2018SW001936.

Jull AJT, Panyushkina IP, Lange TE, Kukarskih VV, Myglan VS, Clark KJ, Salzer MW, Burr GS, Leavitt SW. 2014. Excursions in the ^{14}C record at AD 774–775 in tree rings from Russia and America. *Geophys Res Lett* **41**: 3004–3030. https://doi.org/10.1002/2014GL059874.

Kiefer J. 1990. *Biological radiation effects*. Springer-Verlag, Berlin-Heidelberg. ISBN 978-3-540-510895, 978-3-642-83769-2.

Koldobskiy S, Mekhaldi F, Kovaltsov G, Usoskin I. 2023. Multiproxy reconstructions of integral energy spectra for extreme solar particle events of 7176 BCE, 660 BCE, 775 CE and 994 CE. *J Geophys Res Space Phys* **128(3)**: e2022JA031186. https://doi.org/10.1029/2022JA031186.

Koldobskiy S, Mishev A. 2022. Fluences of solar energetic particles for last three GLE events: Comparison of different reconstruction methods. *Adv Space Res* **70(9)**: 2585–2592. https://doi.org/10.1016/j.asr.2021.11.032.

Koldobskiy S, Raukunen O, Vainio R, Kovaltsov G, Usoskin I. 2021. New reconstruction of event-integrated spectra (spectral fluences) for major solar energetic particle events. *A&A* **647**: A132. https://doi.org/10.1051/0004-6361/202040058.

Koldobskiy SA, Bindi V, Corti C, Kovaltsov GA, Usoskin IG. 2019. Validation of the neutron monitor yield function using data from AMS-02 experiment 2011–2017. *J Geophys Res Space Phys* **124**: 2367–2379. https://doi.org/10.1029/2018JA026340.

Latocha M, Beck P, Rollet S. 2009. AVIDOS-a software package for European accredited aviation Dosimetry. *Radiat Prot Dosim* **136(4)**: 286–290. https://doi.org/10.1093/rpd/ncp126.

Levenberg K. 1944. A method for the solution of certain non-linear problems in least squares. *Q Appl Math* **2**: 164–168.

Lingenfelter R, Ramaty R. 1970. The neutron moderated detector and the determination of rigidity dependence of protons from the September 1–2, 1971 solar flare. In: *Proceedings of the 12th Nobel symposium, Radiocarbon Variations and Absolute Chronology*, Almqvist & Wiksell, Stockholm; Wiley Interscience Division, New York, pp. 513–537.

Marquardt D. 1963. An algorithm for least-squares estimation of nonlinear parameters. *SIAM J Appl Math* **11(2)**: 431–441.

Matthiä D, Heber B, Reitz G, Meier M, Sihver L, Berger T, Herbst K. 2009. Temporal and spatial evolution of the solar energetic particle event on 20 January 2005 and resulting radiation doses in aviation. *J Geophys Res Space Phys* **114(8)**: A08104. https://doi.org/10.1029/2009JA014125.

Matthiä D, Meier M, Schennetten K. 2022. New operational dose quantity ambient dose H* in the context of galactic cosmic radiation in aviation. *J Radiol Prot* **42**: 021520. https://doi.org/10.1088/1361-6498/ac5be0.

Matthiä D, Sihver L, Meier M. 2008. Monte-Carlo calculations of particle fluences and neutron effective dose rates in the atmosphere. *Radiat Prot Dosim* **131(2)**: 222–228. https://doi.org/10.1093/rpd/ncn130.

Meier M, Trompier F, Ambrozova I, Kubancak J, Matthiä D, Ploc O, Santen N, Wirtz M. 2016. CONCORD: Comparison of cosmic radiation detectors in the radiation field at aviation altitudes. *J Space Weather Space Clim* **6**: A24. https://doi.org/10.1051/swsc/2016017.

Meier MM, Copeland K, Matthiä D, Mertens CJ, Schennetten K. 2018. First steps toward the verification of models for the assessment of the radiation exposure at aviation altitudes during quiet space weather conditions. *space weather* **16(9)**: 1269–1276. https://doi.org/10.1029/2018SW001984.

Mertens C, Meier M, Brown S, Norman R, Xu X. 2013. NAIRAS aircraft radiation model development, dose climatology, and initial validation. *Space Weather* **11(10)**: 603–635. https://doi.org/10.1002/swe.20100.

Miroshnichenko L. 2018. Retrospective analysis of GLEs and estimates of radiation risks. *J Space Weather Space Clim* **8**: A52. https://doi.org/10.1051/swsc/2018042.

Mishev A. 2023. Application of the global neutron monitor network for assessment of spectra and anisotropy and the related terrestrial effects of strong SEPs. *J Atmos Sol-Terr Phys* **243**: 106021. https://doi.org/10.1016/j.jastp.2023.106021.

Mishev A, Binios A, Turunen E, Leppänen A-P, Larsen N, Tanskanen E, Usoskin I, Envall J, Iinatti T, Lakkala P. 2022a. Measurements of natural radiation with an MDU Liulin type device at ground and in the atmosphere at various conditions in the Arctic region. *Radiat Meas* **154**: 106757. https://doi.org/10.1016/j.radmeas.2022.106757.

Mishev A, Jiggens P. 2019. Preface to measurement, specification and forecasting of the Solar Energetic Particle (SEP) environment and Ground Level Enhancements (GLEs). *J Space Weather Space Clim* **9**: E1. https://doi.org/10.1051/swsc/2019003.

Mishev A, Kocharov L, Koldobskiy S, Larsen N, Riihonen E, Vainio R, Usoskin I. 2022b. High-resolution spectral and anisotropy characteristics of solar protons during the GLE No 73 on 28 October 2021 derived with neutron-monitor data analysis. *Solar Phys* **297(7)**: 88. https://doi.org/10.1007/s11207-02202026-0.

Mishev A, Koldobskiy S, Kocharov L, Usoskin I. 2021a. GLE # 67 event on 2 November 2003: An analysis of the spectral and anisotropy characteristics using verified yield function and detrended neutron monitor data. *Solar Phys* **296(5)**: 79. https://doi.org/10.1007/s11207-021-01832-2.

Mishev A, Koldobskiy S, Usoskin I, Kocharov L, Kovaltsov G. 2021b. Application of the verified neutron monitor yield function for an extended analysis of the GLE #71 on 17 May 2012. *Space. Weather* **19(2)**: e2020SW002626. https://doi.org/10.1029/2020SW002626.

Mishev A, Mavrodiev S, Stamenov J. 2005. Gamma rays studies based on atmospheric Cherenkov technique at high mountain altitude. *Int J Mod Phys A* **20(29)**: 7016–7019. https://doi.org/10.1142/S0217751X05030727.

Mishev A, Poluianov S. 2021. About the altitude profile of the atmospheric cut-off of cosmic rays: new revised assessment. *Solar Phys* **296(8)**: 129. https://doi.org/10.1007/s11207-021-01875-5.

Mishev A, Tuohino S, Usoskin I. 2018a. Neutron monitor count rate increase as a proxy for dose rate assessment at aviation altitudes during GLEs. *J Space Weather Space Clim* **8**: A46. https://doi.org/10.1051/swsc/2018032.

Mishev A, Usoskin I. 2015. Numerical model for computation of effective and ambient dose equivalent at flight altitudes: Application for dose assessment during GLEs. *J Space Weather Space Clim* **5(3)**: A10. https://doi.org/10.1051/swsc/2015011.

Mishev A, Usoskin I. 2018. Assessment of the radiation environment at commercial jet-flight altitudes during GLE 72 on 10 September 2017 using neutron monitor data. *Space Weather* **16(12)**: 1921–1929. https://doi.org/10.1029/2018SW001946.

Mishev A, Usoskin I, Raukunen O, Paassilta M, Valtonen E, Kocharov L, Vainio R. 2018b. First analysis of GLE 72 event on 10 September 2017: spectral and anisotropy characteristics. *Solar Phys* **293**: 136. https://doi.org/10.1007/s11207-018-1354-x.

Mishev AL, Koldobskiy SA, Kovaltsov GA, Gil A, Usoskin IG. 2020. Updated neutron-monitor yield function: bridging between in situ and ground-based cosmic ray measurements. *J Geophys Res Space Phys* **125(2)**: e2019JA027433. https://doi.org/10.1029/2019JA027433.

Miyake F, Nagaya K, Masuda K, Nakamura T. 2012. A signature of cosmic-ray increase in AD 774–775 from tree rings in Japan. *Nature* **486**: 240–242. https://doi.org/10.1038/nature11123.

Miyake F, Usoskin I, Poluianov S. 2019. *Extreme Solar Particle Storms; The hostile Sun. 2514-3433*. IOP Publishing, Bristol, UK. https://doi.org/10.1088/2514-3433/ab404a. ISBN 978-0-7503-2232-4.

Moraal H, McCracken K. 2012. The time structure of ground level enhancements in solar cycle 23. *Space Sci Rev* **171(1–4)**: 85–95. https://doi.org/10.1007/s11214-011-9742-7.

Nevalainen J, Usoskin I, Mishev A. 2013. Eccentric dipole approximation of the geomagnetic field: Application to cosmic ray computations. *Adv Space Res* **52(1)**: 22–29. https://doi.org/10.1016/j.asr.2013.02.020.

Nuntiyakul W, Sáiz A, Ruffolo D, Mangeard P-S, Evenson P, Bieber J, Clem J, Pyle R, Duldig M, Humble J. 2018. Bare neutron counter and neutron monitor response to cosmic rays during a 1995 latitude survey. *J Geophys Res Space Phys* **123(9)**: 7181–7195. https://doi.org/10.1029/2017JA025135.

Panovska S, Korte M, Constable C. 2019. One hundred thousand years of geomagnetic field evolution. *Rev Geophys* **57(4)**: 1289–1337. https://doi.org/10.1029/2019RG000656.

Paschalis P, Mavromichalaki H, Dorman L, Plainaki C, Tsirigkas D. 2014. Geant4 software application for the simulation of cosmic ray showers in the Earth's atmosphere. *New Astron* **33**: 26–37. https://doi.org/10.1016/j.newast.2014.04.009.

Pelliccioni M. 2000. Overview of fluence-to-effective dose and fluence-to-ambient dose equivalent conversion coefficients for high energy radiation calculated using the FLUKA code. *Radiat Prot Dosim* **88(4)**: 279–297. https://doi.org/10.1093/oxfordjournals.rpd.a033046.

Petoussi-Henss N, Bolch W, Eckerman K, Endo A, Hertel N, Hunt J, Pelliccioni M, Schlattl H, Zankl M. 2010. Conversion coefficients for radiological protection quantities for external radiation exposures. *Ann ICRP* **40(2–5)**: 1–257.

Picone JM, Hedin AE, Drob DP, Aikin AC. 2002. NRLMSISE-00 empirical model of the atmosphere: statistical comparisons and scientific issues. *J Geophys Res Space Phys* **107(12)**: 1468. https://doi.org/10.1029/2002JA009430.

Poluianov S, Usoskin I, Mishev A, Shea M, Smart D. 2017. GLE and sub-GLE redefinition in the light of high-altitude polar neutron monitors. *Solar Phys* **292(11)**: 176. https://doi.org/10.1007/s11207-017-1202-4.

Potgieter M. 2013. Solar modulation of cosmic rays. *Living Rev Solar Phys* **10**: 3. https://doi.org/10.12942/lrsp-2013-3.

Pulkkinen T. 2007. Space weather: terrestrial perspective. *Living Rev Solar Phys* **4(1)**: 1–60. https://doi.org/10.12942/lrsp-2007-1.

Reames D. 2013. The two sources of solar energetic particles. *Space Sci Rev* **175(1–4)**: 53–92. https://doi.org/10.1007/s11214-013-9958-9.

Schwenn R. 2006. Space weather: the solar perspective. *Living Rev Solar Phys* **3**: 1. https://doi.org/10.12942/lrsp-2006-2.

Shea M, Smart D. 1982. Possible evidence for a rigidity-dependent release of relativistic protons from the solar corona. *Space Sci Rev* **32**: 251–271. https://doi.org/10.1007/BF00225188.

Shea M, Smart D. 2000. Fifty years of cosmic radiation data. *Space Sci Rev* **93(1–2)**: 229–262. https://doi.org/10.1023/A:1026500713452.

Shea M, Smart D. 2012. Space weather and the ground-level solar proton events of the 23rd solar cycle. *Space Sci Rev* **171**: 161–188. https://doi.org/10.1007/s11214-012-9923-z.

Simpson J. 2000. The cosmic ray nucleonic component: the invention and scientific uses of the neutron monitor. *Space Sci Rev* **93**: 11–32. https://doi.org/10.1023/A:1026567706183.

Spurny F, Dachev T. 2001. Measurements in an aircraft during an Intense solar flare, ground level event 60, on April 15, 2001. *Radiat Prot Dosim* **95(3)**: 273–275. https://doi.org/10.1093/oxfordjournals.rpd.a006552.

Spurny F, Dachev T, Kudela K. 2002. Increase of onboard aircraft exposure level during a solar flare. *Nuclear Energy Safety* **10(48)**: 396–400.

Sukhodolov T, Usoskin I, Rozanov E, Asvestari E, Ball WT, et al. 2017. Atmospheric impacts of the strongest known solar particle storm of 775 AD. *Sci Rep* **7**: 45257. https://doi.org/10.1038/srep45257.

Tikhonov A, Goncharsky A, Stepanov V, Yagola A. 1995. *Numerical methods for solving ill-posed problems*. Kluwer Academic Publishers, Dordrecht. ISBN 978-90-481-4583-6.

Tuohino S, Ibragimov A, Usoskin I, Mishev A. 2018. Upgrade of GLE database: assessment of effective dose rate at flight altitude. *Adv Space Res* **62(2)**: 398–407. https://doi.org/10.1016/j.asr.2018.04.021.

Usoskin I. 2017. A history of solar activity over millennia. *Living Rev Solar Phys* **14**: 3. https://doi.org/10.1007/s41116-017-0006-9.

Usoskin I, Alanko-Huotari K, Kovaltsov G, Mursula K. 2005. Heliospheric modulation of cosmic rays: monthly reconstruction for 1951–2004. *J Geophys Res* **110**: A12108. https://doi.org/10.1029/2005JA011250.

Usoskin I, Gil A, Kovaltsov G, Mishev A, Mikhailov V. 2017. Heliospheric modulation of cosmic rays during the neutron monitor era: calibration using PAMELA data for 2006–2010. *J Geophys Res* **122**: 3875–3887. https://doi.org/10.1002/2016JA023819.

Usoskin I, Koldobskiy S, Kovaltsov G, Gil A, Usoskina I, Willamo T, Ibragimov A. 2020a. Revised GLE database: fluences of solar energetic particles as measured by the neutron-monitor network since 1956. *A&A* **640**: 2038272. https://doi.org/10.1051/0004-6361/202038272.

Usoskin IG, Koldobskiy SA, Kovaltsov GA, Rozanov EV, Sukhodolov TV, Mishev AL, Mironova IA. 2020b. Revisited reference solar proton event of 23 February 1956: assessment of the cosmogenic-isotope method sensitivity to extreme solar events. *J Geophys Res Space Phys* **125(6)**: e2020JA027921. https://doi.org/10.1029/2020JA027921.

Usoskin IG, Kovaltsov GA. 2021. Mind the gap: new precise 14C data indicate the nature of extreme solar particle events. *Geophys Res Lett* **48(17)**: e2021GL094848. https://doi.org/10.1029/2021GL094848.

Usoskin IG, Kromer B, Ludlow F, Beer J, Friedrich M, Kovaltsov GA, Solanki SK, Wacker L. 2013. The AD775 cosmic event revisited: the Sun is to blame. *A&A* **552**: L3. https://doi.org/10.1051/0004-6361/201321080.

Usoskin IG, Solanki SK, Krivova N, Hofer B, Kovaltsov GA, Wacker L, Brehm N, Kromer B. 2021. Solar cyclic activity over the last millennium reconstructed from annual ^{14}C data. *A&A* **649**: A141. https://doi.org/10.1051/0004-6361/202140711.

Uusitalo J, Arppe L, Hackman T, Helama S, Kovaltsov G, et al. 2018. Solar superstorm of AD 774 recorded subannually by Arctic tree rings. *Nat Commun* **9(1)**: 3495. https://doi.org/10.1038/s41467-01805883-1.

Vainio R, Desorgher L, Heynderickx D, Storini M, Flückiger E, et al. 2009. Dynamics of the Earth's particle radiation environment. *Space Sci Rev* **147(3–4)**: 187–231. https://doi.org/10.1007/s11214-009-9496-7.

Vashenyuk E, Balabin Y, Miroshnichenko L. 2008. Relativistic solar protons in the ground level event of 23 February 1956: New study. *Adv Space Res* **41(6)**: 926–935. https://doi.org/10.1016/j.asr.2007.04.063.

Vashenyuk E, Balabin Y, Perez-Peraza J, Gallegos-Cruz A, Miroshnichenko L. 2006. Some features of the sources of relativistic particles at the Sun in the solar cycles 21–23. *Adv Space Res* **38(3)**: 411–417. https://doi.org/10.1016/j.asr.2005.05.012.

Vos E, Potgieter M. 2015. New modeling of galactic proton modulation during the minimum of solar cycle 23–24. *Astrophys J* **815**: 119. https://doi.org/10.1088/0004-637X/815/2/119.

Yang Z, Sheu R. 2020. An in-depth analysis of aviation route doses for the longest distance flight from Taiwan. *Radiat Phys Chem* **168**: 108548. https://doi.org/10.1016/j.radphyschem.2019.108548.

Appendix

A.1. Event-integrated ambient dose

In the appendix, we present global maps of the event-integrated ambient doses during 774 AD extreme SEP event assuming worst case Figure A.1 and a realistic scenario Figure A.2. The altitude dependence of the event-integrated H* for the conservative and realistic scenarios is given as an animated gif in the electronic supplement. We note, that differences in event-integrated ambient doses are more pronounced at an altitude of 35 kft (10.7 km) a.s.l., because of the reduced secondary particle flux, accordingly dose, and the selected color scheme.

The event-integrated ambient doses allow one to study the event on a global scale and can be used as a reference to study worst-case space weather effects.

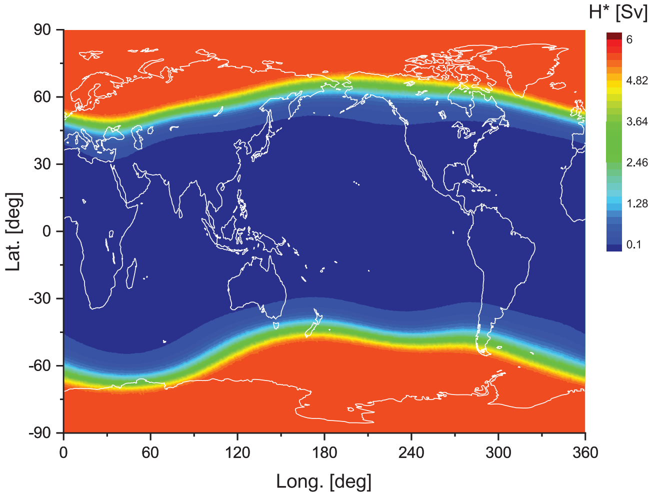

Figure A.1. Global map of the event-integrated ambient dose at altitude 40 kft (12.2 km) during 774 AD event, assuming worst case scenario.

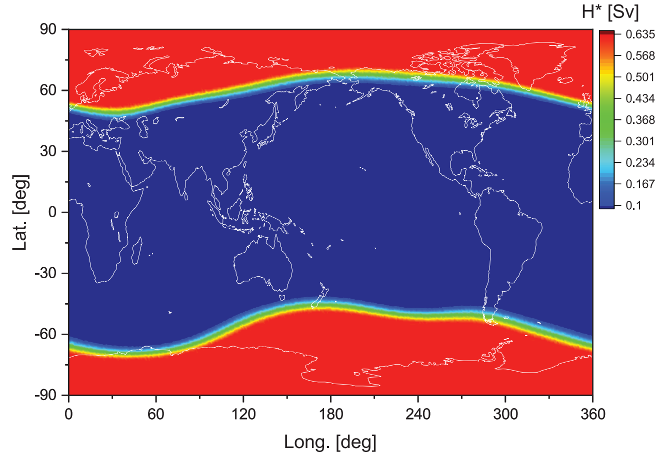

Figure A.2. Global map of the event-integrated ambient dose at altitude 40 kft (12.2 km) during 774 AD event, assuming realistic case scenario.

Cite this article as: Mishev A, Panovska S & Usoskin I 2023. Assessment of the radiation risk at flight altitudes for an extreme solar particle storm of 774 AD. *J. Space Weather Space Clim.* **13**, 22. https://doi.org/10.1051/swsc/2023020.